ELSEVIER

Journal of Nuclear Materials 290–293 (2001) 407–412

journal of nuclear materials

www.elsevier.nl/locate/jnucmat

Reversal of in–out asymmetry of the particle-recycling associated with *X*-point MARFE and plasma detachment

A. Hatayama [a,*], H. Segawa [a], N. Komatsu [a], R. Schneider [b], D.P. Coster [c], N. Hayashi [d], S. Sakurai [d], N. Asakura [d]

[a] *Faculty of Science and Technology, Keio University, 3-14-1 Hiyoshi, Kouhoku-ku, Yokohama 223–8522, Japan*
[b] *Max-Planck-Institut für Plasmaphysik, EURATOM-Association, D-17489 Greifswald, Germany*
[c] *Max-Planck-Institut für Plasmaphysik, EURATOM-Association, D-85748 Garching, Germany*
[d] *Naka Fusion Research Establishment, Japan Atomic Energy Research Institute, Ibaraki 311-0193, Japan*

Abstract

Reversal of in–out asymmetry of the particle recycling in tokamak divertor regions and its physical mechanism have been studied. Numerical calculations by the 'B2-EIRENE' code have been done for the JT-60U open divertor geometry. The following two cases, $n_D = 1.0 \times 10^{19}$ m^{-3} and $n_D = 2.0 \times 10^{19}$ m^{-3} for the D^+ ion density at the core interface boundary, have been calculated. In the high-density case, typical behaviors of *X*-point MARFE and plasma detachment have been observed. In addition, asymmetry of the particle recycling between the inner and the outer divertor regions is reversed in comparison with the low-density case. The difference of the electron temperature between the inner and the outer regions together with the T_e-dependence of the ionization rate coefficient is shown to be a possible cause of the reversal of the recycling source. Also, the difference of pressure loss between two regions plays a key role in the in–out asymmetry of the particle flux at the plate.

Keywords: B2/EIRENE; Detachment; Divertor plasma; Divertor asymmetry; JT-60U; MARFE; Particle flux; Particle recycling

1. Introduction

Control of the divertor heat load and target plate erosion is one of the most critical and important issues for the achievement of long pulse and steady-state tokamak operation. In order to reduce the heat and particle loads on the divertor plates to a manageable level, several ways have been proposed up to now. Among them, the detached plasma operation mode is one of the most possible candidates for future fusion reactors [1].

However, since the detached plasma state favors the high plasma density and low power reaching the target, the plasma detachment from the divertor plate is often associated with MARFE phenomena [2]. The MARFEs often appear in the high-density operation of tokamaks close to the so-called upper density limit and are characterized by strong increases in the radiation loss in the plasma edge region. In case of strong radiation power loss around the *X*-point in the diverted tokamaks due to MARFE, it is often called the *X*-point MARFE.

Recently, the reversal of in–out asymmetry of the divertor particle recycling at the onset of the *X*-point MARFE and/or plasma detachment has been observed in several tokamak divertor experiments [3–5]. However, its physical mechanism is not yet adequately clear. In the present paper, numerical calculations by the B2-Eirene code [6–8] have been done for the JT-60U open divertor geometry with the discharge parameter range of relatively low power and L-mode experiments [9] to understand the possible causes of the reversal.

* Corresponding author. Tel.: +81-45 563 1141; fax: +81-45 563 0322.
E-mail address: akh@ppl.appi.keio.ac.jp (A. Hatayama).

0022-3115/01/$ - see front matter
PII: S0022-3115(00)00639-5

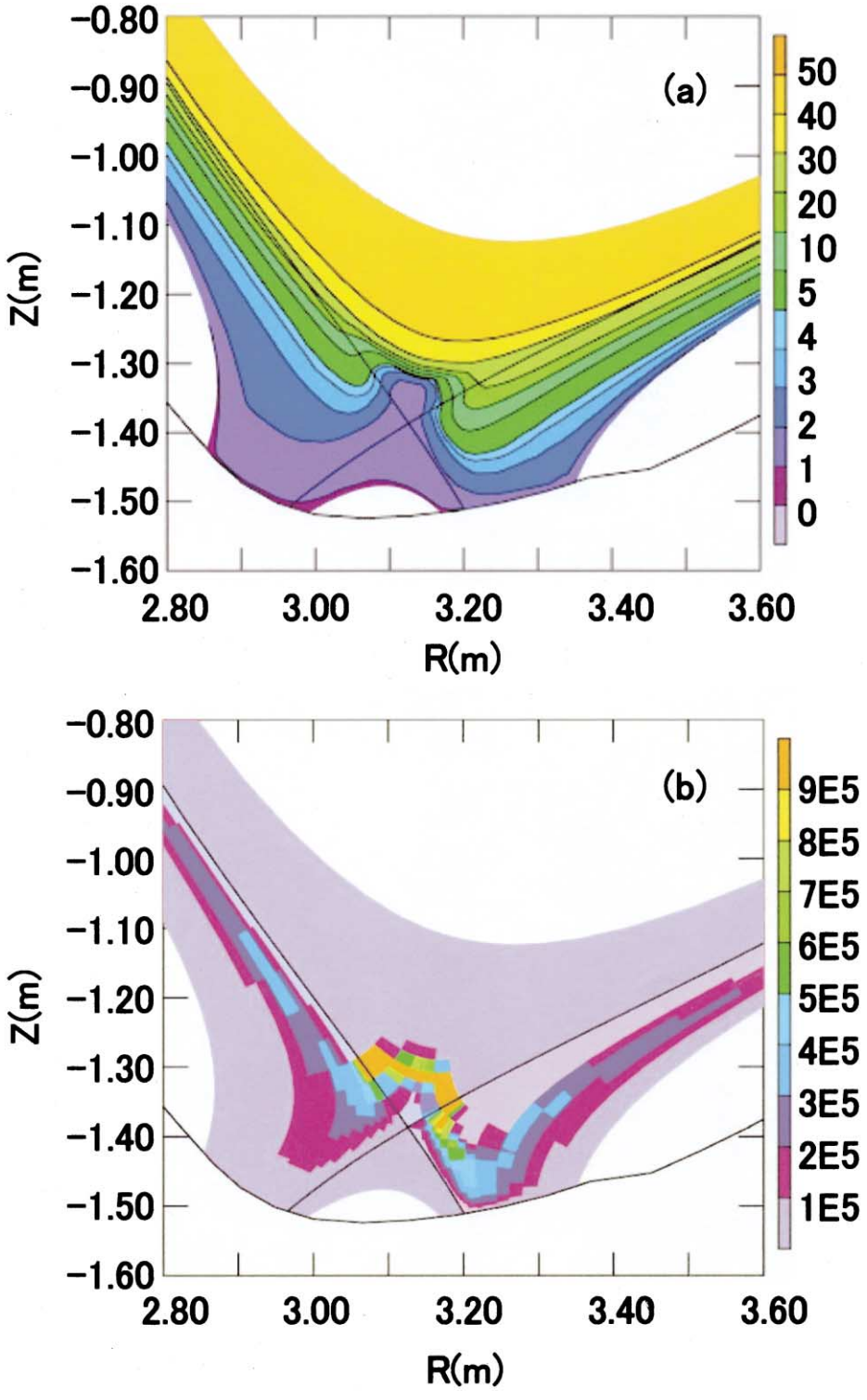

Fig. 1. Results of (a) electron temperature (eV) and (b) total radiation power (W/m^3) from carbon impurities for the high-density case (Case B: $n_D^{core} = 2.0 \times 10^{19}$ m^{-3}). 2D spatial profiles near the X-point and divertor region in the poloidal cross-section.

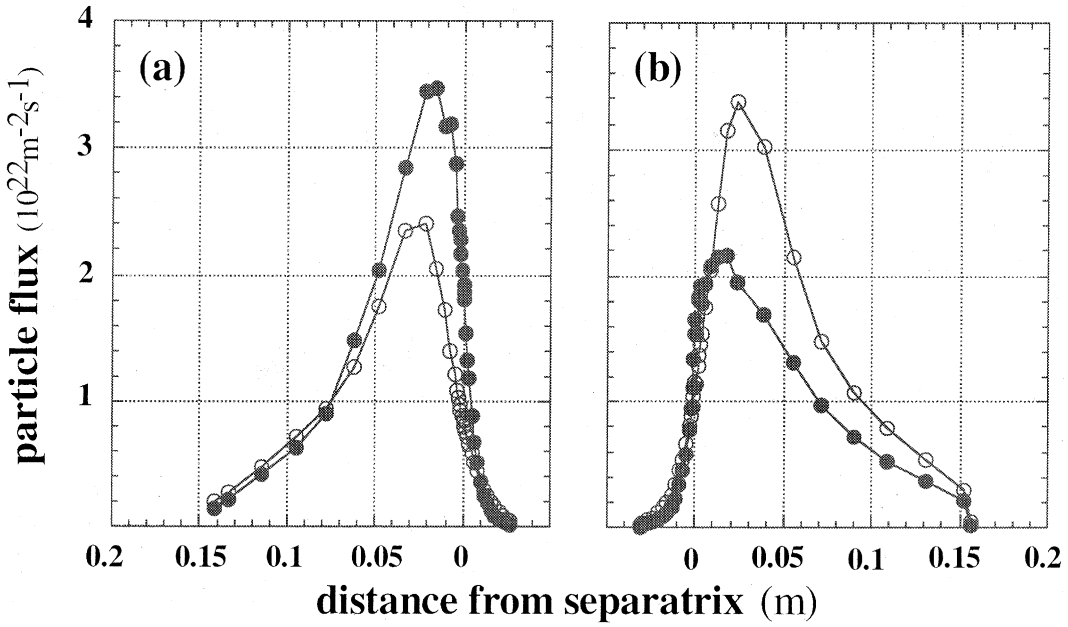

Fig. 2. Particle flux at the target plate as a function of the distance from the separatrix: (a) the inner target and (b) the outer target. (●) are the results for the low-density case (Case A: $n_D^{core} = 1.0 \times 10^{19} m^{-3}$), while (○) are those for the high-density case (Case B: $n_D^{core} = 2.0 \times 10^{19}$ m^{-3}).

2. Numerical model

The 'B2-EIRENE' code package has been applied to the analyses for many present tokamak experiments and the predictive study for the future reactors. The main aspects of the B2-EIRENE code are described in detail in [6–8]. Here, we briefly summarize the numerical model and the main assumptions used in the application of the code for this study.

Bulk ion species D^+ and all carbon impurity ion species, C^+–C^{6+}, are considered and are described in the fluid approximation by the 'B2' multi-fluid code [6]. This plasma description by the B2 fluid code is self-consistently coupled to the 'EIRENE' Monte Carlo code[7] for the neutrals. Essential features of neutral dynamics for D, D_2 and C are taken into account by the EIRENE code. The numerical grid used for study is generated from a JT-60U MHD equilibrium of shot #E24830. This shot is one of typical large volume and L-mode discharges of JT-60U. The basic plasma parameters of this shot are as follows [9]: the plasma current was $I_p = 1.8$ MA, the toroidal magnetic field $B_t = 3.5$ T, and the effective safety factor $q_{eff} = 4.7$. At the core interface boundary (CIB) i.e., at the innermost flux surface of the grid inside the separatrix, a total energy input of 2.5 MW equally split between the ion and electron channel is assumed. At the CIB, the bulk ion density n_D is also fixed. The following two cases are calculated: Case A (low-density case): $n_D^{core} = 1.0 \times 10^{19}$ m^{-3}, Case B (high-density case): $n_D^{core} = 2.0 \times 10^{19}$ m^{-3}. The remaining boundary conditions are the standard ones and kept fixed throughout this study.

As for the parallel transport, classical transport coefficients have been used in the present study as usual in the most of the 2D edge plasma simulations. With respect to the cross-field transport, however, there still exist relatively large uncertainties. In the present study, anomalous transport with constant heat diffusivity ($\chi_{e\perp} = \chi_{i\perp} = 2.0$ m^2/s) has been used for the electron and the ion energy balance equations. For the particle balance equations, the cross-field particle fluxes have been given in the form as $\Gamma_\perp = nv_{out} - D_\perp \partial n/\partial x$. In addition to the anomalous diffusion with the constant diffusion coefficient ($D_\perp = 0.3$ m^2/s), an artificial outward velocity v_{out} is considered, representing the possibility of strongly enhanced turbulent transport due to the onset of flute-like turbulence with loss of line tying [10]. Qualitatively good fit has been obtained for the upstream SOL features in the experiments.

3. Numerical results

In the low-density case (Case A: $n_D^{core} = 1.0 \times 10^{19}$ m^{-3}), a typical high recycling state has been reached at the inner side divertor. The electron temperature T_e decreases and the electron density n_e increases along the field line toward the target plate. The

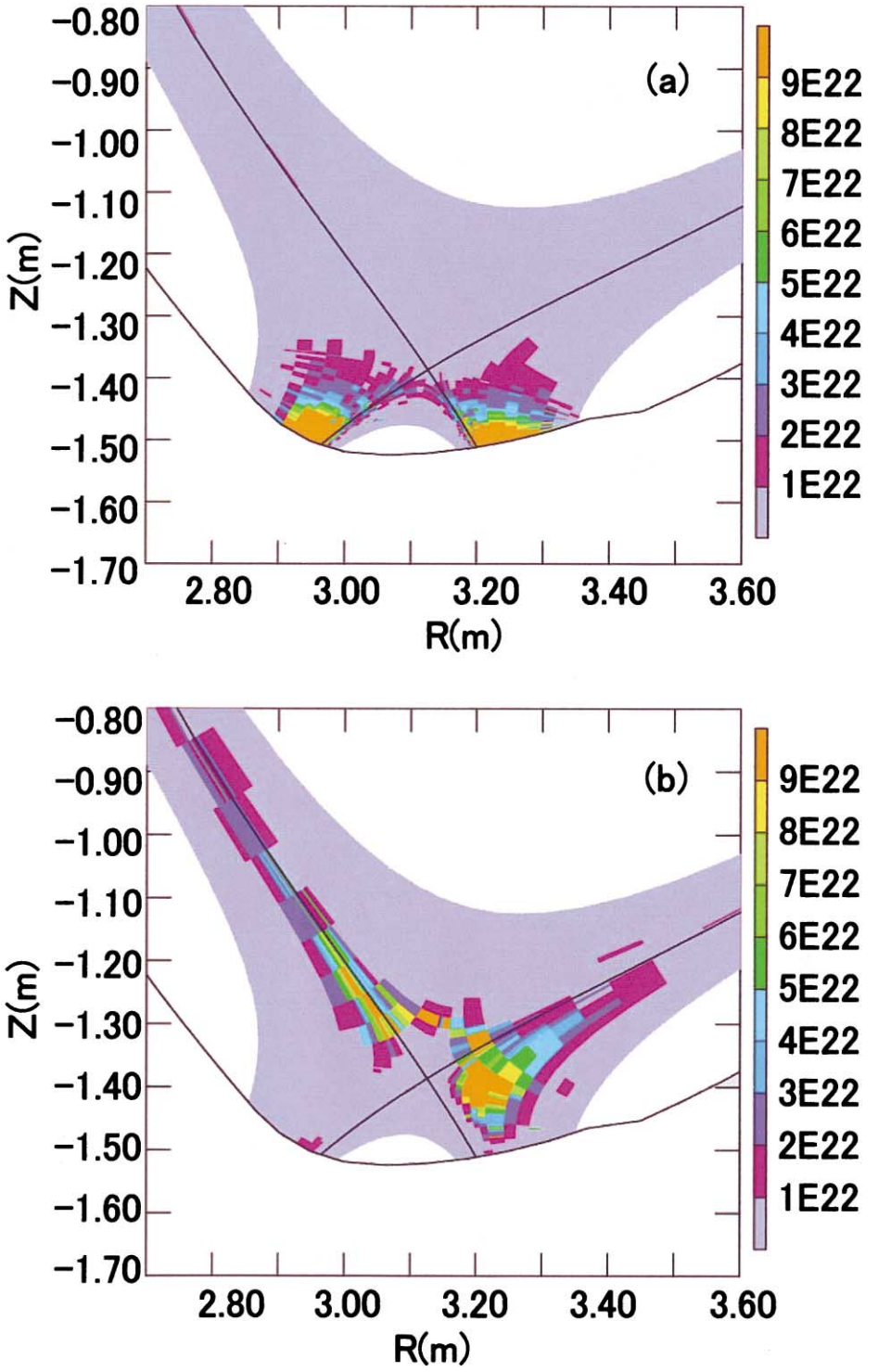

Fig. 3. 2D spatial distribution of the hydrogen ionization source S_i (D^+ions/m^3/s). Comparison between (a) Case A ($n_D^{core} = 1.0\times 10^{19}$ m^{-3}) and (b) Case B ($n_D^{core} = 2.0 \times 10^{19}$ m^{-3}).

outer side divertor region is still in the low recycling state. Near the separatrix hit point of the inner plate, T_e and n_e becomes as $T_e \sim 15$ eV and $n_e \sim 3.5 \times 10^{19}$ m^{-3}, while $T_e \sim 35$ eV and $n_e \sim 1.5 \times 10^{19}$ m^{-3} at the outer plate. In comparison with the above features in the low-density case, T_e and n_e profiles have quite different features in the high-density case (Case B: $n_D^{core} = 2.0 \times 10^{19}$ m^{-3}). Fig. 1(a) shows 2D spatial profile of T_e (eV) near the divertor region. Typical characteristics of *X*-point MARFE can be seen in this case. A low temperature region locally exists inside the separatrix just above the *X*-point. Fig. 1(b) shows the 2D spatial profile of the carbon line radiation power for Case B. The impurity radiation near the *X*-point becomes large in this high-density case. On the other hand, the impurity-radiated region is mainly localized still in the divertor region below the *X*-point for Case A. The fraction of the total radiation power from carbon and hydrogen to the input power (2.5 MW) in the low-density case is about 30%. However, in the high-density case with the *X*-point MARFE, it becomes very large and is about 65% of the total input power.

In the low-density case, the total power reached to the inner and to the outer divertor plate is about 700 and 550 kW, respectively. In this case, the total plasma pressure is almost constant along the field line and both divertor plasmas are in the attached state. On the other hand, in the high-density case with the *X*-point MARFE, the power load to the plate is greatly reduced and only about 200 and 150 kW are reached to the inner and the outer plates, respectively. The electron temperatures in both divertor regions are quite low as shown in Fig. 1(a). The *X*-point MARFE in the high-density case is accompanied by the plasma detachment.

Figs. 2(a) and (b) show the particle flux at the inner and outer target plates. It is shown as a function of the distance from the separatrix. The closed circles are the results for the low-density case, while the open circles are those for the high-density case. The reversal of in–out asymmetry of the particle flux is clearly seen. In Figs. 3(a) and (b), the 2D spatial profiles of the hydrogen ionization source (D^+ions/m^3/s) are compared between (a) Case A and (b) Case B. In Case B with the *X*-point MARFE, the ionization front moves upward off the target plate. The recycling source in the outer divertor region is clearly larger than in the inner divertor region.

The ionization source, $S_i = n_e n_0 \langle \sigma v \rangle$, depends on n_e, neutral density n_0 and T_e through the ionization rate coefficient $\langle \sigma v \rangle$. For $T_e < 10$ eV, $\langle \sigma v \rangle$ decreases quite rapidly with T_e decreasing and this T_e-dependence of $\langle \sigma v \rangle$ is important to understand the tendency in Fig. 3. Fig. 4 shows 1D spatial profiles of T_e along a field line that passes through nearly the peak of the heat flux at the target plate. The horizontal axis is the grid number along the field line. The vertical lines correspond to the height of the *X*-point in 2D geometry. At both low

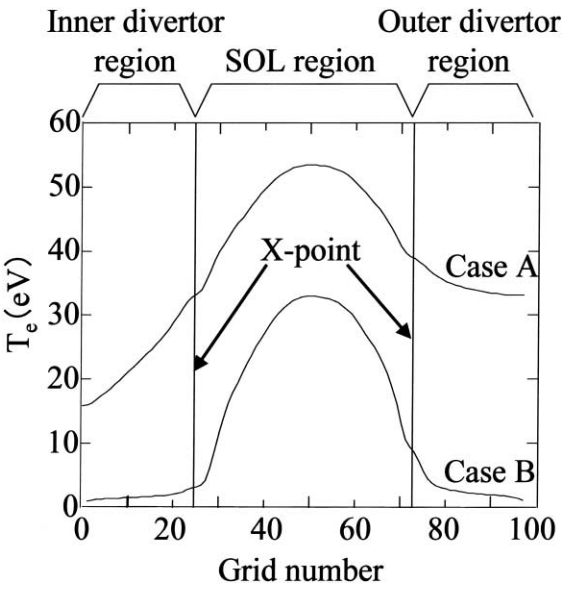

Fig. 4. 1D spatial profile of electron temperature along a field line is plotted as a function of the grid number N from the inner target plate ($N = 0$) to the outer target plate ($N = 97$). Comparison between the low-density case (Case A: $n_D^{core} = 1.0 \times 10^{19}$ m^{-3}) and (b) the high-density case (Case B: $n_D^{core} = 2.0 \times 10^{19}$ m^{-3}).

density (Case A) and high density (Case B), the inner divertor is colder than the outer. This is mainly due to the fact that power entering the outer SOL across the separatrix Q^{out} is larger than that which enters the inner SOL Q^{in} (Case A: $Q^{out}/Q^{in} = 1.9$, Case B: $Q^{out}/Q^{in} = 1.8$). For Case A, $T_e \sim 15$–35 eV in the inner divertor region and $T_e \sim 35$–40 eV in the outer region. In this T_e-range, the dependence of $\langle \sigma v \rangle$ on T_e is not so large as below 10 eV. On the other hand, for Case B, T_e largely decreases in both regions. However, near the entrance of the outer divertor region, i.e., near the outer *X*-point, T_e is still high enough ($T_e \sim 10$eV) for the ionization, while T_e is less than 3 eV for almost the entire region of the inner divertor. For $T_e < 10$ eV, $\langle \sigma v \rangle$ decreases quite rapidly with T_e decreasing as mentioned above and $\langle \sigma v \rangle$ for $T_e \sim 10$ eV is about two orders of magnitude larger than that for $T_e \sim 3$ eV. As a result, the recycling source in the outer region for Case B becomes larger than that in the inner region as shown in Fig. 3. This leads to the reversal of in–out asymmetry of the particle recycling between the low-density and the high-density cases, i.e., with and without the *X*-point MARFE.

As pointed out in [11,12], plasma pressure loss due to ion-neutral friction becomes important for reducing particle flux for $T_e < 5$ eV. In order to discuss our numerical results from the above view point of pressure loss, here, we introduce a ratio $\Gamma_d^{in}/\Gamma_d^{out}$, where Γ_d^{in} and Γ_d^{out} are the particle fluxes to the outer plate and the inner plate along the same flux tube. The particle flux at

the plate is given by $\Gamma_d = n_d C_s = p_d/\sqrt{m_i k T_d}$, where n_d, C_s, k, m_i and T_d are the plasma density, the isothermal sound speed, Boltzmann constant, the ion mass and the sum of ion and electron temperature ($T_d = T_d^i + T_d^e$), respectively. Then, $\Gamma_d^{out}/\Gamma_d^{in}$ becomes as $\Gamma_d^{in}/\Gamma_d^{out} = (p_d^{in}/p_d^{out})\sqrt{T_d^{out}/T_d^{in}}$, where p_d^{in}/p_d^{out} is the pressure ratio between the inner and outer divertor plates. As an example, we take the position where the flux becomes the maximum (about 2 cm from the separatrix) in Figs. 2(a) and (b). For Case A (closed circle), $\Gamma_d^{in}/\Gamma_d^{out}$ becomes 1.61 at this position from Fig. 2. In this low-density case, pressure is almost conserved along the field line and the pressure ratio is $p_d^{in}/P_d^{out} = 0.95$, while $\sqrt{T_d^{out}/T_d^{in}} = 1.69$ and the inner divertor is colder than the outer. As a result, the flux ratio becomes as $\Gamma_d^{in}/\Gamma_d^{out} = 1.61$, i.e., the colder inner divertor experiences higher ion particle flux than the outer divertor ($\Gamma_d^{in}/\Gamma_d^{out} > 1$) as shown in Fig. 2. On the other hand, at high density (Case B: open circle), $p_d^{in}/p_d^{out} = 0.53$, $\sqrt{T_d^{out}/T_d^{in}} = 1.34$ and these values lead to $\Gamma_d^{in}/\Gamma_d^{out} = 0.71$ in Fig. 2. In this high-density case, the inner and outer divertor temperatures drop to the point where ion-neutral friction becomes important. From Figs. 1(a) and 4, the temperature is somewhat colder at the inner divertor and therefore the amount of pressure loss along the field lines can become larger there. Thus, the plasma pressure at the inner plate is reduced from that at the outer plate ($p_d^{in}/p_d^{out} = 0.53 < 1$). This results in a reduction of particle flux at the inner plate in comparison to the outer plate ($\Gamma_d^{in}/\Gamma_d^{out} < 1$) and also the reversal of the asymmetry of the particle flux at the plate in comparison with Case A ($\Gamma_d^{in}/\Gamma_d^{out} > 1$).

4. Conclusion and future study

Numerical calculations by the B2-EIRENE code have been done for the JT-60U open divertor geometry with the parameter range of L-mode discharges. In the high-density case, the reversal of in–out asymmetry of the particle recycling associated with X-point MARFE is observed in the simulation as in the experiments. In comparison with the low-density case, T_e in the divertor region largely decreases and $T_e < 3$ eV in the inner region. However, at the entrance of the outer divertor region, T_e is still relatively high ($T_e \sim 10$ eV). This difference of T_e between the inner and the outer regions together with the T_e-dependence of the ionization rate coefficient is shown to be a possible cause of the reversal of in–out asymmetry of the recycling source. In addition, it is shown that the difference of pressure loss between two regions in the plasma detachment plays a key role in the in–out asymmetry of the particle flux at the divertor plate.

Numerical study for the W-shaped divertor in JT-60U is now underway. The results and detailed comparisons with those for the open geometry will be reported elsewhere. In addition, effects of drifts and current have not yet been taken into account. These effects are important for the SOL and divertor characteristics, especially, for the asymmetric properties. In the future, these effects will be also taken into account in the analyses.

References

[1] ITER Physics expert group, Nucl. Fus. 39 (1999) 2391.
[2] B. Lipschutz, J. Nucl. Mater. 145–147 (1987) 15.
[3] N. Asakura et al., Nucl. Fus. 36 (1996) 795.
[4] A. Loarte et al., Nucl. Fus. 38 (1998) 331.
[5] H. Tamai et al., J. Plasma Fus. Res. 74 (1998) 1336.
[6] B.J. Braams et al., Fus. Technol. 9 (1986) 320.
[7] D. Reiter et al., J. Nucl. Mater. 196–198 (1992) 80.
[8] R. Schneider et al., J. Nucl. Mater. 196–198 (1992) 810.
[9] N. Asakura et al., J. Nucl. Mater. 241–242 (1992) 559.
[10] H.S. Bosch et al., J. Nucl. Mater. 220–222 (1995) 558.
[11] P.C. Stangeby, Nucl. Fus. 33 (1993) 1695.
[12] C.S. Pitcher, P.C. Stangeby, Plasma Phys. Control. Fus. 39 (1997) 779.